EAST EUROPEAN JOURNAL OF PHYSICS. 4. 31-42 (2021)
DOI: 10.26565/2312-4334-2021-4-03 ISSN 2312-4334

THE EFFECT OF HYDROSTATIC PRESSURE AND CATIONIC VACANCY ON THE ELECTRONIC AND MAGNETIC PROPERTIES OF THE ZnSe:T CRYSTALS (T = Ti, V, Cr, Mn, Fe, Co, Ni)[†]

Stepan V. Syrotyuk
Semiconductor Electronics Department, Lviv Polytechnic National University, 12 S. Bandera Str., 79013 Lviv Ukraine
**Corresponding Author: svsnpe@gmail.com*
Received August 7, 2021; revised November 17, 2021; accepted November 18, 2021

The parameters of the spin-polarized electronic energy spectrum of ZnSe:T crystals (T = Ti, V, Cr, Mn, Fe, Co, Ni) are studied on the basis of a 2 × 2 × 2 supercell built on the basis of a ZnSe unit cell with a sphalerite structure. The supercell contains 64 atoms, with one Zn atom replaced by one transition 3d element T. The first stage of this study is to calculate in the ideal material ZnTSe parameters of electronic energy bands, dependent on the external hydrostatic pressure. At the second stage, the effect of pressure on the parameters of the electronic energy spectrum in the ZnTSe materials is investigated, taking into account the Zn vacancy. The calculations were performed using the Abinit program. For a better description of strongly correlated 3d electrons of the element T, a hybrid exchange-correlation functional PBE0 with an admixture of the Hartree-Fock exchange potential was used, in which the self-interaction error of these electrons is removed. Based on the obtained spin-polarized electron densities of states, the magnetic moments of the supercells were also determined. A significant effect of pressure on the parameters of electronic energy zones was revealed. So, the ideal ZnTiSe material at zero pressure is a metal for both spin values, but under pressure it becomes a semiconductor. The same material with a point defect, i.e. a vacancy at the site of the Zn atom, exhibits semiconductor properties for both spin orientations at zero pressure. It was found that vacancies radically change the parameters of electronic energy bands. The magnetic moments of the supercell, as integral values of the spin-polarized densities of electronic states, also reflect these changes. Thus, in ZnTiSe material without defects, the magnetic moments of the supercell are 1.92, 2.0 and 2.0 μ_B, at pressures 0, 21 and 50 GPa, respectively, while in the same material with a vacancy, the corresponding values are 0.39, 0.02 and 0.36 μ_B. The ideal ZnVSe material at zero pressure is also a metal for both values of the spin moment, but in the presence of a cationic vacancy it is characterized by a pseudogap because the Fermi level is localized in the upper part of the valence band. Ideal ZnFeSe and ZnNiSe crystals are characterized by similar dependences of the electronic energy parameters on the pressure, for both spins. However, the same materials with a cationic vacancy are characterized by the Fermi level immersed in the valence band for a spin up.
Keywords: ZnSe, 3d impurity, cationic vacancy, electronic properties, spin, magnetic moment, strong correlations, hybrid functional.
PACS: 68.35.Dv, 71.15.Mb, 71.20.Nr, 71.27.+a, 81.05.Bx

The ultrashort pulse lasers of infrared (IR) light have gained great attentions for ophthalmic, surgical, dental, therapeutic, and aesthetic medical applications. The pulses from the picosecond (ps) to femtosecond (fs) require less energy to ablate biological tissues and the accuracy is in the micrometer range. The passively mode-locked femtosecond ZnSe:Cr laser was first reported in 2006, generating ~100 fs pulses at up to 75 mW power around 2.5 μm wavelength [1].

ZnSe is a wide band gap semiconductor, widely used in light-emitting devices, solar cells, and photodetectors because of its high excitation energy and excellent photoelectric performance [2]. The optical and electrical properties of semiconductor materials are the main factors that determine the performance of devices. At present, it is the most widely used way to regulate the photoelectric characteristics of semiconductors through morphology regulation or doping treatment. The doping technique by introducing donor impurities or acceptor impurities into the host lattice is one of the most effective ways to achieve regulatory effects, and it can accurately control the transport properties of the semiconductor by adjusting the type of doping element and the doping concentration. In addition, the mechanism of the change of optical and conductive properties of ZnSe caused by doping has not been studied deeply in theory.

The ZnS:Cr lasers have been extensively studied both experimentally and theoretically. The zinc-blende ZnS has the larger band gap of 3.8 eV, higher thermal conductivity of 27 W/mK, higher thermal shock parameter of 7.1 $W/m^{1/2}$, and lower dn/dT of $46 \cdot 10^{-6}$ K^{-1}, compared respectively to 2.8 eV, 18 W/mK, 5.3 $W/m^{1/2}$, and $70 \cdot 10^{-6}$ K^{-1} in ZnSe [3].

The physical, spectroscopic, and laser characteristics of the single crystal and polycrystalline II-VI chalcogenides are practically identical [4]. This is important since II-VI single-crystals of high optical quality are difficult to grow while chemically vapor grown II-VI polycrystals benefited from low-cost mass production technology of fabrication and were widely used as passive materials for middle-infrared technology [5]. The combination of low-cost and readily available polycrystalline II-VI materials with a quantitative and affordable post-growth TM doping procedure, preserving high optical quality of the starting materials, enabled an effective technology for fabrication of gain elements, which is quite rare for solid-state laser materials.

Since ZnS, ZnSe, ZnTe crystals with impurities of transition 3d elements are used in devices, particular in lasers, it is important to study their electronic structure from the unified theoretical methodology under the action of hydrostatic

[†] ***Cite as:*** S.V. Syrotyuk, East. Eur. J. Phys. **4**, 31 (2021), https://doi.org/10.26565/2312-4334-2021-4-03

pressure and vacancies at the site of the zinc atom. The aim of this study is also to take into account the strong correlations of 3d electrons using a hybrid exchange-correlation functional. Let us go to performing these tasks.

CALCULATION

We solve the Schrödinger equation in the basis of projectior augmented waves (PAW) [6], which combines the features of the pseudopotential approaches [7] and the all-electronic method of augmented plane waves (APW) [8]. In the PAW and APW methods, the crystal is divided into two regions. The first region is inside the atomic spheres, and the second one is interspherical. In the APW approach, the wave functions of both regions are joining at the surface of the sphere to ensure continuity throughout space. In the PAW method, an augmentation is performed using a projection procedure.

The all-electronic wave $|\psi_n>$ and pseudo-wave $|\tilde{\psi}_n>$ functions are connected as follows [6]:

$$|\psi_n(\mathbf{r})> = |\tilde{\psi}_n(\mathbf{r})> + \sum_a \sum_i (|\phi_i^a(\mathbf{r})> - |\tilde{\phi}_i^a(\mathbf{r})>) < \tilde{p}_i^a | \tilde{\psi}_n >, \tag{1}$$

where $|\phi_i^a(\mathbf{r})>$ is atomic wave, $|\tilde{\phi}_i^a(\mathbf{r})>$ pseudo-wave, and $<\tilde{p}_i^a|$ projector function, respectively. The summation in (1) is performed by the augmentation spheres, which are numbered by the index a, and the index $i = \{n, l, m\}$ incorporates the principal, orbital and magnetic quantum numbers, respectively.

From equation (1) we see that

$$|\psi_n(\mathbf{r})> = \tau |\tilde{\psi}_n(\mathbf{r})>, \tag{2}$$

where the τ operator converts a pseudo-wave $|\tilde{\psi}_n(\mathbf{r})>$ into an all-electron wave function $|\psi_n(\mathbf{r})>$.

The explicit form of the operator τ follows from equation (1):

$$\tau = 1 + \sum_a \sum_i (|\phi_i^a> - |\tilde{\phi}_i^a>) < \tilde{p}_i^a|. \tag{3}$$

Stationary Schrödinger equation

$$H|\psi_n> = \varepsilon_n |\psi_n>, \tag{4}$$

taking into account (2) takes the following form [4]:

$$\tau^+ H \tau |\tilde{\psi}_n> = \tau^+ \tau |\tilde{\psi}_n> \varepsilon_n, \tag{5}$$

in which the required electron spectrum ε_n is the same as in equation (4).

The idea of the PAW method is to convert the Schrödinger equation to an equation in which the unknown state function is $|\tilde{\psi}_n>$. If it is found, then with the help of (1) the all-electronic wave function is obtained. Through the latter we find the electron density and the corresponding Hartree potential.

The exchange-correlation potential was chosen in the form of PBE0 [9–12], according to which the exchange-correlation energy

$$E_{xc}^{PBE0}[\rho] = E_{xc}^{PBE}[\rho] + \alpha(E_x^{HF}[\psi_{3d}] - E_x^{PBE}[\rho_{3d}]), \tag{6}$$

where PBE corresponds to the generalized gradient approximation (GGA-PBE) of exchange-correlation functional [12], and $E_x^{HF}[\psi_{3d}]$ is the exchange energy in the Hartree-Fock theory. The recommended value of a mixing factor α is equal to $1/4$. In formula (6), the exchange energy $E_x^{PBE}[\rho_{3d}]$, in which the self-interaction error (SIE) of 3d electrons is the largest, is partially subtracted. In fact, these electrons move in narrow energy bands with a high density of states. In the included exact term of exchange energy $E_x^{HF}[\psi_{3d}]$ the SIE is absent in general. Neglecting the second term in formula (6) leads to a conventional GGA-PBE exchange-correlation functional suitable for describing materials with s (p) electrons.

The functional $E_{xc}^{PBE0}[\rho]$ is important for describing materials containing d (f) electrons. In particular, it has been successfully used to study nanostructures containing transition 3d elements [13, 14]. Energy band structure peculiarities and luminescent parameters of CeX_3 (X = Cl, Br, I) crystals were revealed and shown good comparison with experiment [15]. Electronic properties of orthorhombic InI and TlI crystals taking into account the quasiparticle corrections and spin-orbit interaction, have been evaluated based on the results, defined at the level of the hybrid functional as the starting point [16]. The combined approach of the hybrid functional and quasiparticle GW was successfully used in the calculations of the electronic structure in chalcogenides ZnX (X=O, S, Se, Te) [17]. The results obtained in works [16, 17] are in good agreement with experimental data. The electronic structure of the CdMnTe solid solution [18] is satisfactory agreed with the experimental results [19]. Electronic structure, magnetic and mechanical properties of MnCoSi half-Heusler alloy also have been found with the hybrid PBE0 exchange-correlation functional [20], where the different values of the mixing coefficient α were used.

All calculations were performed using the ABINIT program [21], in 2 × 2 × 2 supercells containing 64 atoms. At the first stage, the defect of substitution in the supercell $Zn_{32}Se_{32}$ of one Zn atom by transition element T, i.e. $Zn_{31}T_1Se_{32}$ is considered. At the second stage the supercell with a vacancy, $Zn_{30}v_1T_1Se_{32}$, is treated. The electronic structure of these materials was calculated under the action of hydrostatic pressure.

The calculations are performed on the basis of PAW. The following valence configurations of atoms were selected: Zn: $3d^{10}4s^2$, Se: $4s^24p^4$, Ti: $3s^23p^63d^24s^2$, V: $3s^23p^63d^34s^2$, Cr: $3s^23p^63d^54s^1$, Mn: $3s^23p^63d^54s^2$, Fe: $3s^23p^63d^64s^2$, Co: $3s^23p^63d^74s^2$, and Ni: $3s^23p^63d^84s^2$. Basic functions and pseudopotentials (PAW) were generated using AtomPAW code [22, 23]. The calculation of the wave function was performed on the basis of plane waves determined by the maximum kinetic energy ε_{cut} = 40 Ry, on a spatial grid of 90×90×90. Electron density and potentials were calculated on a denser grid of 125 × 125 × 125, determined by an energy ε_{cut} = 80 Ry.

RESULTS AND DISCUSSION

The spin-polarized electron energies in the ZnTiSe material are shown in Fig. 1. The parameters of the electronic energy band spectrum are denoted as follows: E_v - the energy of the top of the valence band, E_f - the Fermi energy, E_c - the lowest electron energy in the conduction band. Figures 1a and 1b show the electron energies in an ideal ZnSe crystal in which one Zn atom is replaced by a Ti atom. The parameters of supercell 2×2×2, which contains 64 atoms, correspond to the applied external pressures from 0 to 50 GPa. In other words, the value of the constant lattice for the supercell $a = 19.14$ Å corresponds to the pressure P = 50 GPa, and the value of $a =$ 21.64 Å corresponds to the pressure 0 GPa, i.e. to ambient conditions.

Note that under normal conditions (P = 0) the ZnTiSe material exhibits metallic properties for both spin orientations, i.e. $\varepsilon_g = 0$. The magnetic moment of the supercell $M = 1.92\,\mu_B$. However, under the action of hydrostatic pressure, this material reveals the properties of a semiconductor for both spins. Increasing the hydrostatic pressure leads to an increase in the width of the band gap ε_g, as it is shown in Figures 1a and 1b. At a pressure value of $P = 21$ GPa for spin up, the direct optical gap at the point Γ $\varepsilon_{gd} = 0.72$ eV, and the fundamental indirect one $\varepsilon_{gi} = 0.61$ eV.

For the spin down, the optical direct gap is identical with the fundamental one, and the numerical value is $\varepsilon_g = 2.19$ eV. Magnetic moment of the supercell $M = 2.0\,\mu_B$. At a pressure $P = 50$ GPa, for spin up, the direct optical gap at the Γ point $\varepsilon_{gd} =$ 0.69 eV, and the fundamental indirect one $\varepsilon_{gi} = 0.54$ eV. For the spin down, the optical and fundamental band gaps are equal, and the numerical value of $\varepsilon_g =$ 2.03 eV. Magnetic moment of the supercell $M = 2.0\,\mu_B$. As can be seen from Figs. 1a, 1b, and the Fermi level is located inside the forbidden gap.

However, the presence of a point defect, i.e. a vacancy at the Zn atom site, leads to a significant change in the dependence of the electronic energy spectrum in the ZnTiSe material on the external hydrostatic pressure. From Figures 1c and 1d, we see that for both spin orientations, the ZnTiSe material with a point defect exhibits semiconductor properties for all hydrostatic pressure values. At a pressure value $P = 0$, for the spin up, the optical gap at the point Γ $\varepsilon_{gd} = 0.20$ eV, and the fundamental indirect one $\varepsilon_{gi} = 0.18$ eV. For spin down, the optical gap $\varepsilon_{gd} =$ 0.71 eV, and the fundamental indirect one $\varepsilon_{gi} =$ 0.70 eV. The magnetic moment of the supercell $M = 0.39\,\mu_B$. At a pressure value of $P =$ 20 GPa, for the spin up, the optical gap at the point Γ $\varepsilon_{gd} = 0.38$ eV, and the fundamental indirect one $\varepsilon_{gi} =$ 0.35 eV. For spin down, the optical pap $\varepsilon_{gd} = 0.40$ eV, and the fundamental indirect one $\varepsilon_{gi} = 0.37$ eV. The magnetic moment of the supercell $M = 0.02\,\mu_B$. At a pressure value of 48 GPa, for the spin up, the optical gap at a point Γ $\varepsilon_{gd} = 0.43$ eV, and the fundamental indirect one $\varepsilon_{gi} = 0.38$ eV. For the spin down, the optical gap $\varepsilon_{gd} = 0.43$ eV, and the fundamental indirect one $\varepsilon_{gi} = 0.38$ eV. The magnetic moment of the supercell $M = 0.36\,\mu_B$. The largest band gap ε_g is expected under normal conditions for electrons with spins down. For this state, the band gap ε_g decreases with increasing pressure (decrease in the constant lattice of the crystal) from 0 to about 20 GPa, after which its values remain almost constant for both spin orientations, including the pressure value of 48 GPa.

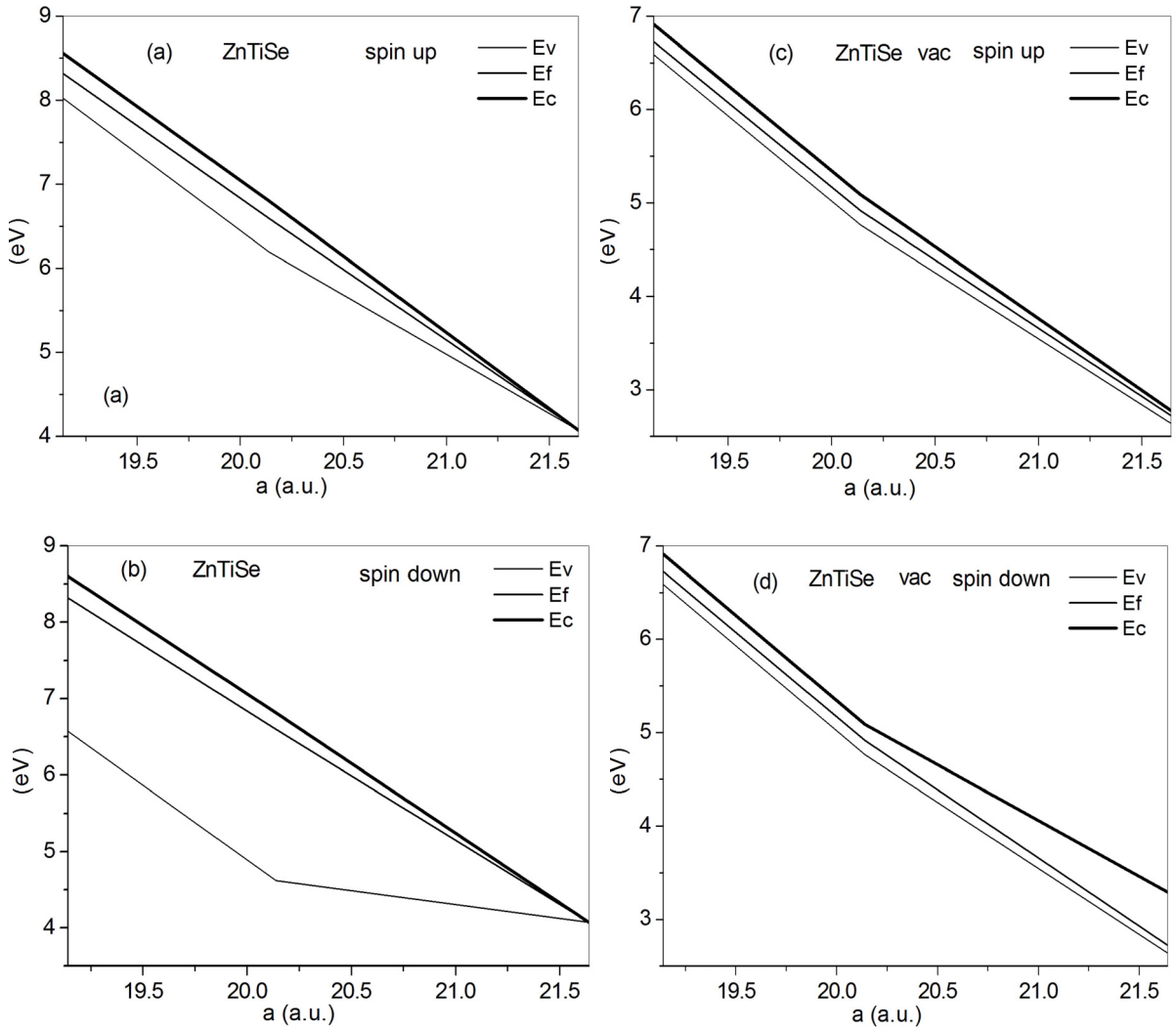

Figure 1. The spin-polarized electronic energy band parameters in the ZnTiSe material versus the 2×2×2 supercell lattice constant: top of valence band E_v, Fermi energy E_f and bottom of conduction band E_c.

The calculation results for the ZnVSe material are shown in Fig. 2. First, consider the parameters of an ideal crystal shown in Figures 2a and 2b. For a pressure $P = 0$, the material reveals a metallic state with a band gap $\varepsilon_g = 0$ for both spin values. The magnetic moment of the supercell $M = 2.7\,\mu_B$. However, at higher pressures, $0 < P \le 21$ GPa, and for states with spin up $E_v = E_c$, i.e. we again have a metallic state. For pressures $21 < P \le 50$ GPa, in states with spin up $E_f < E_v < E_c$, i.e. the Fermi level is localized in the valence band. On the contrary, for spin-down electronic states, the ZnVSe crystal is a semiconductor whose fundamental interband gap $\varepsilon_g = 0$ at a pressure $P = 0$, and for higher pressures $0 < P \le 21$ GPa it increases. At a pressure $P = 21$ GPa, the optical and fundamental gaps are the same, i.e. $\varepsilon_g = 2.20$ eV for both spin orientations. The value of the magnetic moment of the supercell $M = 3\,\mu_B$. At higher pressures, i.e. in the interval $21 < P \le 50$ GPa, the interband gap is almost constant, and the Fermi level is shifted toward the conduction band. At a pressure of 50 GPa, the optical and fundamental slits are the same, i.e. $\varepsilon_g = 1.99$ eV for both spin orientations. The magnetic moment of a supercell $M = 3\,\mu_B$.

If there is a vacancy, we have another picture, shown in Figures 2c and 2d. In fig. 2c we see that for states with spin up, at pressure $P = 0$, the Fermi level is localized inside the band gap, and in the upper part of the valence band at higher pressures. At a pressure of $P = 0$ we have a direct band gap ε_g =1.10 eV at a point Γ. At pressures of 20 and 48 GPa, the values of the pseudogaps are 1.25 and 1.14 eV, respectively. At pressures of 0, 20 and 48 GPa, the magnetic moments of the supercell are 2.7, 3.0 and 3.0 μ_B, respectively.

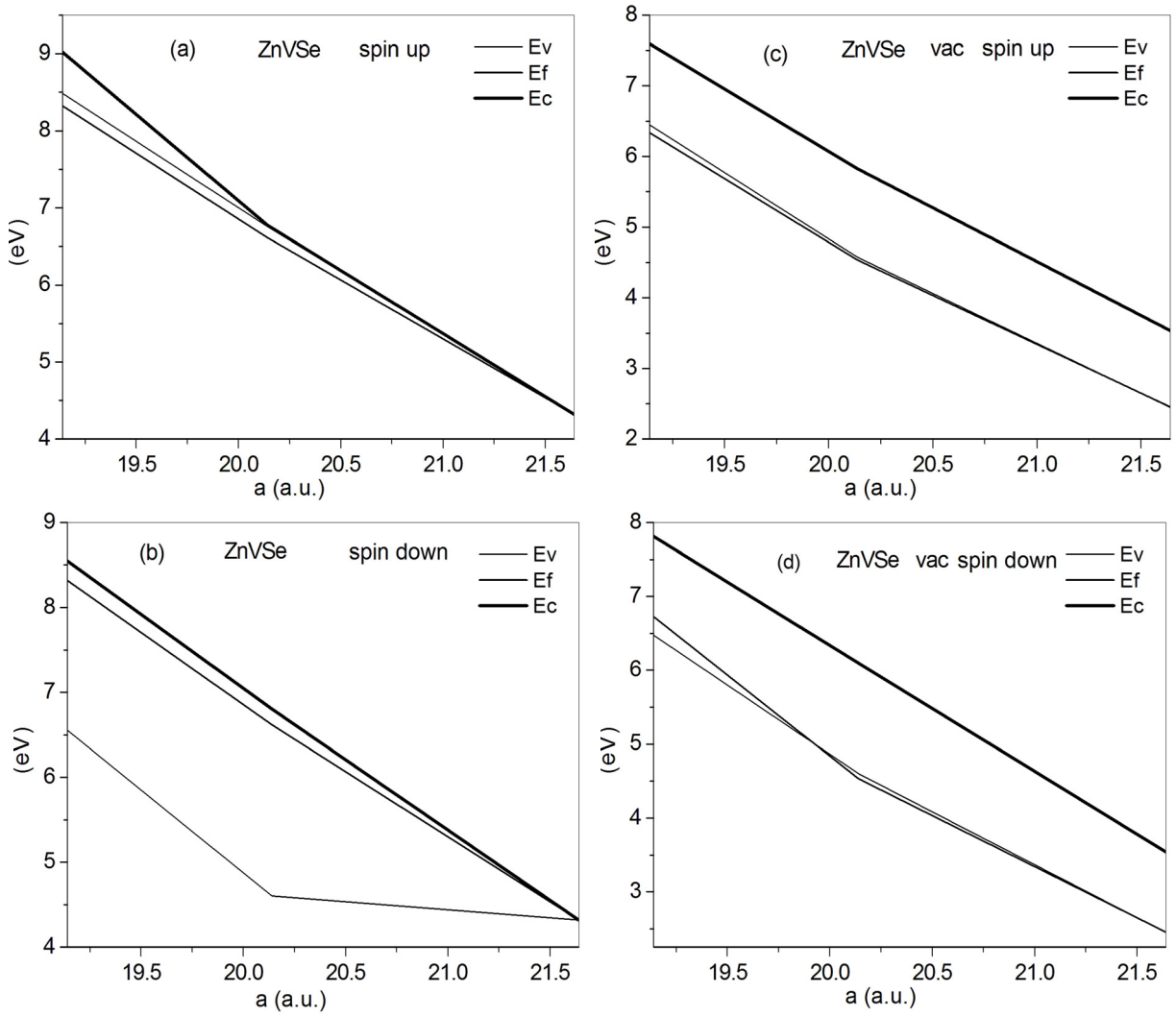

Figure 2. The spin-polarized electronic energy band parameters in the ZnVSe material versus the 2×2×2 supercell lattice constant: top of valence band E_v, Fermi energy E_f and bottom of conduction band E_c.

If there is a vacancy, we have another picture, shown in Figures 2c and 2d. In Fig. 2c we see that for states with spin up at pressure $P = 0$ the Fermi level is localized inside the band gap, and in the upper part of the valence band at higher pressures. At a pressure of $P = 0$ we have a direct band gap ε_g =1.10 eV at a point Γ. At pressures of 20 and 48 GPa, the values of the pseudogaps are 1.25 and 1.14 eV, respectively. At pressures 0, 21 and 50 GPa, the magnetic moments of the supercell are 2.7, 3.0 and 3.0 μ_B, respectively.

For electrons with spin down (Fig. 2 d), under pressure $P = 0$, we have a direct band gap ε_g =1.12 eV at a point Γ. At $0 < P \le 20$ GPa pressures, the Fermi level is localized at the top of the valence band, and the pseudogap value is 1.50 eV if $P = 20$ GPa. At $20 < P \le 48$ GPa pressures, the ZnVSe material with the vacancy is a semiconductor with a band gap of $\varepsilon_g = 1.33$ eV ($P = 48$ GPa). At pressures 0, 20 and 48 GPa, the magnetic moments of the supercell are 2.00, 2.05 and 2.05 μ_B, respectively.

The parameters of the ZnCrSe material E_v, E_f and E_c, depending on the pressure, differ from those shown in Figures 1 and 2 above. Let us first consider the results obtained for an ideal ZnCrSe crystal. They are shown in Figures 3a and 3b. For the spin up (Fig. 3a) we notice the immersion of the Fermi level in the valence band. The interband pseudogap increases with increasing pressure. For the spin down we have a semiconductor, the width of the band gap of which increases with increasing pressure. At pressure values of 0, 22 and 51 GPa, the magnetic moment of the supercell is the same and equal to 4 μ_B, and the values of the optical and fundamental gaps coincide and are 1.20, 2.22 and 1.99 eV, respectively.

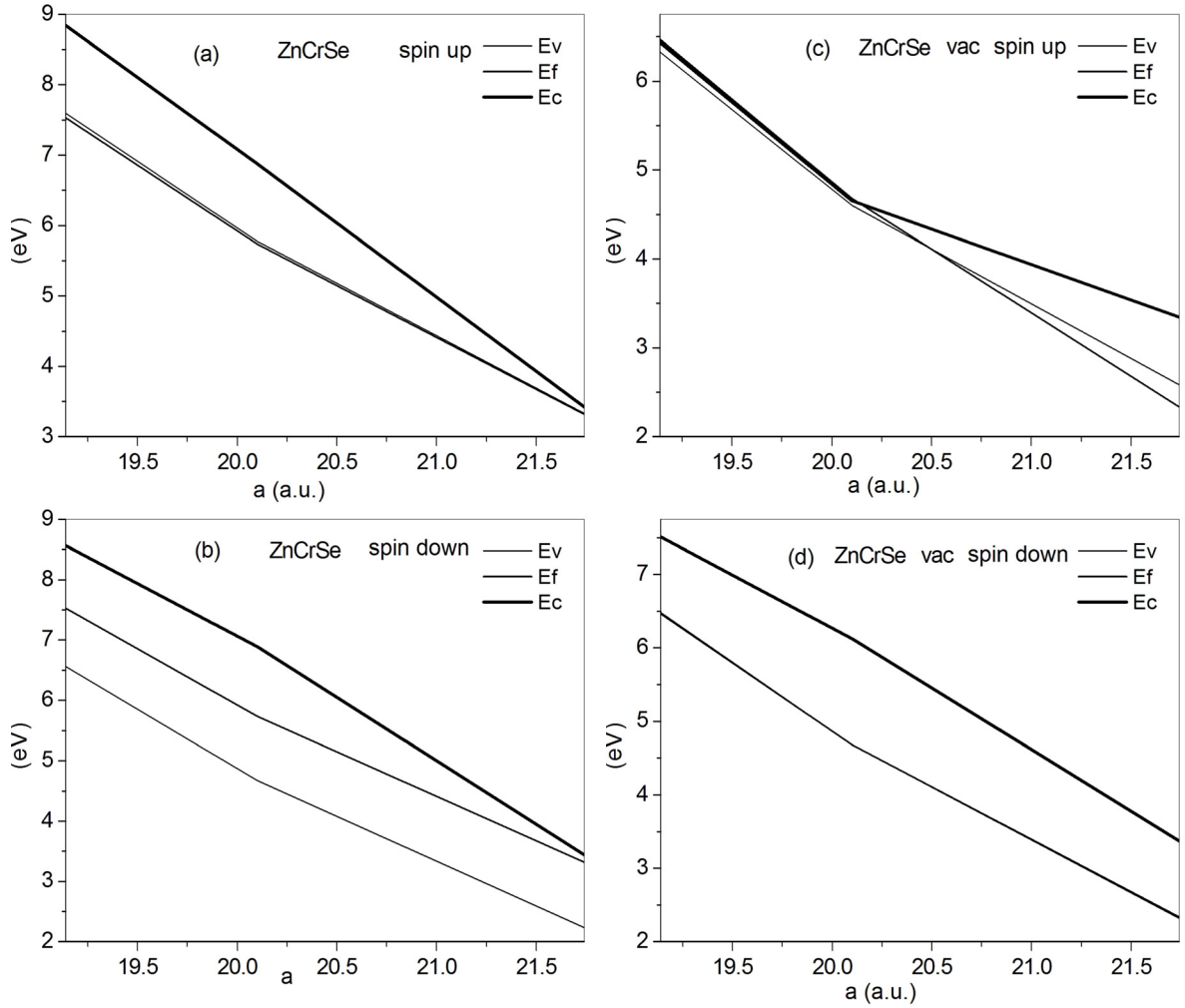

Figure 3. The spin-polarized electronic energy band parameters in the ZnCrSe material versus the 2×2×2 supercell lattice constant: top of valence band E_v, Fermi energy E_f and bottom of conduction band E_c.

Now consider the results obtained for a ZnCrSe crystal with a vacancy at the Zn atom site. At $0 < P \le 22$ GPa pressures, the Fermi level of electrons with spin up (Fig. 3c) is localized in the valence band, and the width of the pseudogap increases. A further increase in pressure leads the material to a metallic state. For electrons with spin down (Fig. 3d), the Fermi level is in the upper part of the valence band, and the pseudogap shows a slow change as a function of pressure. The values of pseudogaps at pressures 0, 20 and 49 GPa are 1.06 eV (optical and fundamental), 1.50 eV (optical) and 1.46 eV (indirect fundamental), and 0 eV, respectively. The magnetic moments of the supercell corresponding to these pressures are equal to 2.75, 2.57 and 2.37 μ_B, respectively.

The pressure-dependent parameters of the electronic energy spectrum of an ideal ZnMnSe material are shown in Figures 4a and 4b. Their change, if there is a vacancy, is shown in Figures 4c and 4d. In an ideal material at pressures of 0, 22 and 51 GPa, the optical band gaps coincide with the fundamental ones, and their values are 1.04, 1.96 and 1.85 eV for spin up, and 1.20, 2.21 and 1.95 eV for spin down, respectively. The magnetic moments of the supercell are the same for these pressure values and are equal to $5\,\mu_B$. Figures 4a and 4b indicate that for both spin up and down, the material is a semiconductor whose band gap slowly increases with increasing in pressure to 22 GPa, and a further increase in pressure causes a slow decrease in bandwidth.

In the presence of a vacancy at the Zn atom site, the picture changes radically. The Fermi level for both spin orientations is at the top of the valence band. At pressures of 0, 20 and 49 GPa, the values of pseudogaps 1.03, 1.96 and 1.85 eV for spin up, and 1.20, 2.07 and 1.55 eV for spin down, respectively. The values of the magnetic moments of the supercell at these values of pressure are equal to 4.16, 4.2 and 4 μ_B, respectively.

The parameters of the electronic energy bands in the ZnFeSe material, depending on the pressure, found without taking into account the vacancy, are shown in Figures 5a, 5b. For spin-up states, we have a direct-band material with interband gaps of 1.14, 1.83, and 1.94 eV, at corresponding pressure values of $P = 0$, 15, and 49 GPa. The increase in pressure leads to a gradual lowering of the Fermi level in the band gap, i.e. it shifts towards the top of the valence band (Fig. 5a).

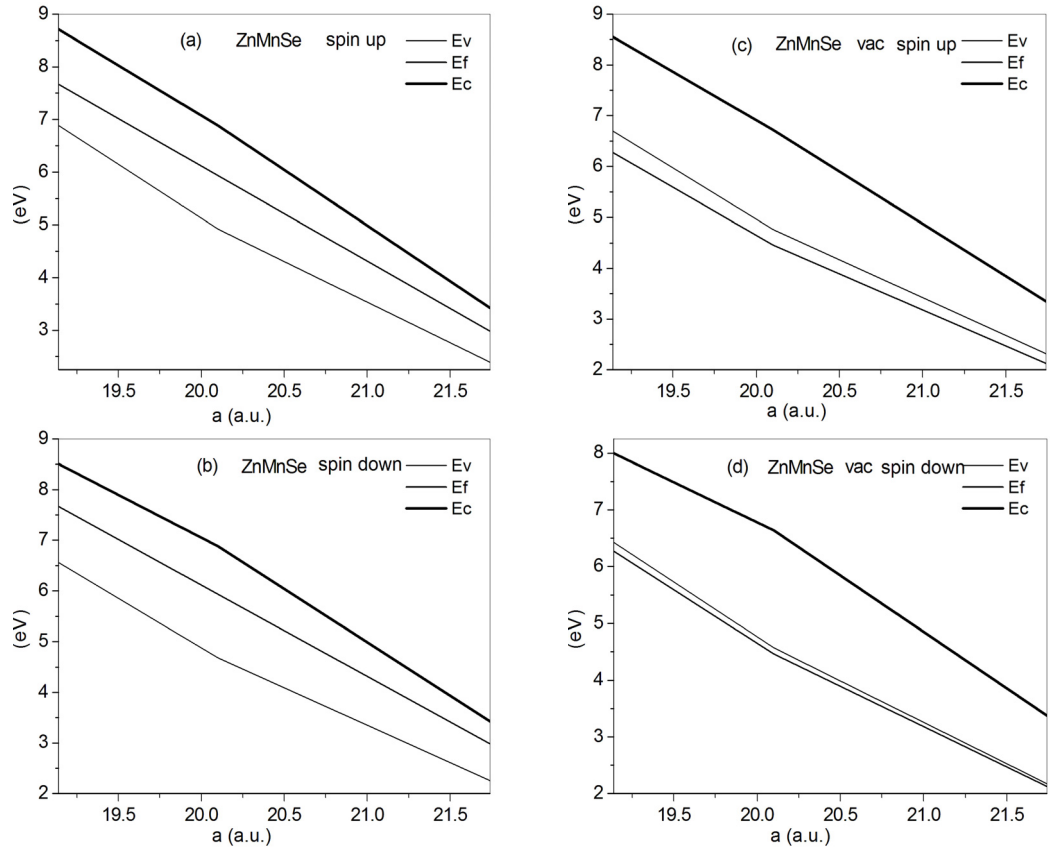

Figure 4. The spin-polarized electronic energy band parameters in the ZnMnSe material versus the 2×2×2 supercell lattice constant: top of valence band E_v, Fermi energy E_f and bottom of conduction band E_c.

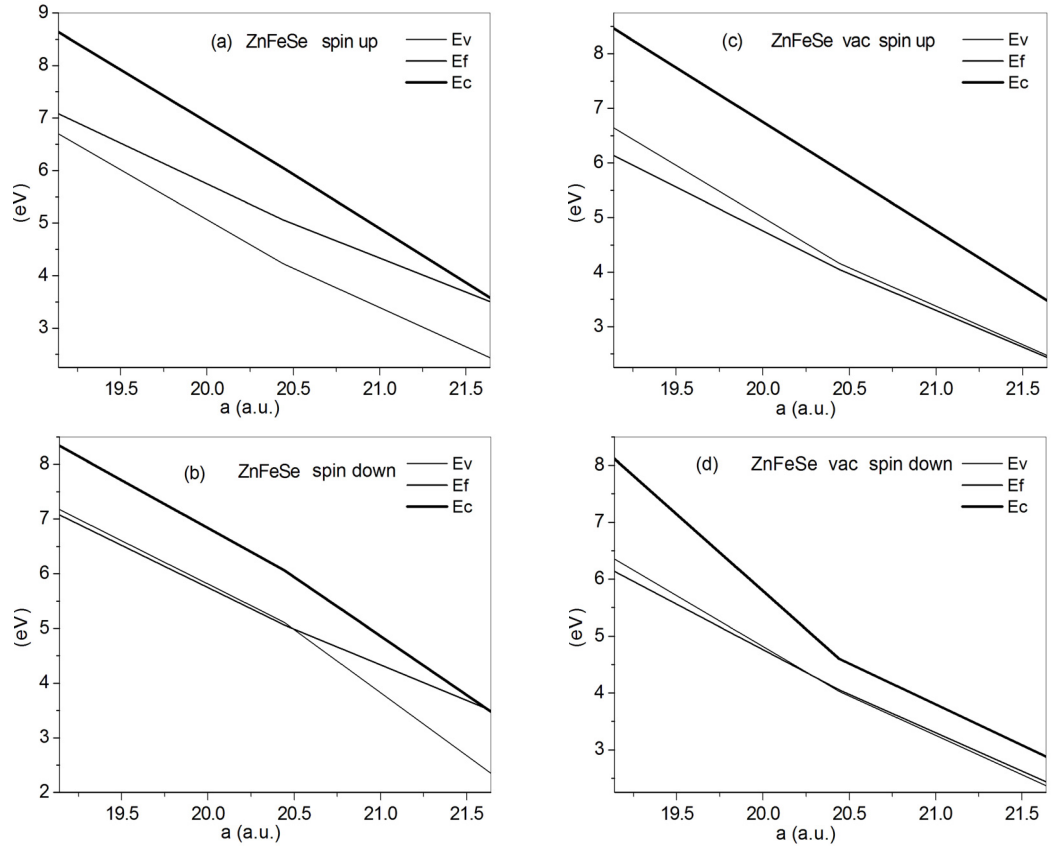

Figure 5. The spin-polarized electronic energy band parameters in the ZnFeSe material versus the 2×2×2 supercell lattice constant: top of valence band E_v, Fermi energy E_f and bottom of conduction band E_c.

A completely different picture is observed for the states of the electron with the spin down. At a pressure value of 0, the Fermi level is in the conduction band, and the pseudogap equals to 1.13 eV. An increase in pressure leads to a decrease in the Fermi level and its immersion in the valence band. The latter occurs at a pressure of $P = 15$ GPa, at which the pseudogap is 0.96 eV. A further increase in pressure leads to a slow increase in the pseudogap to 1.17 eV. The magnetic moment of the supercell at all pressure values $P = 0$, 14 та 47 GPa equals to $M = 4\ \mu_B$.

The presence of a vacancy radically changes the parameters of electronic energy zones. For the spin up, the Fermi level is in the valence band, and at pressure values of $P = 0$, 14, and 47 GPa, the values of the pseudogaps are 1.01, 1.71, and 1.82 eV, respectively.

For spin down at $0 < P \le 14$ GPa pressures, the material is a semiconductor with an optical gap of 0.59 eV and a fundamental indirect one of 0.53 eV. The increase in pressure leads to a slow growth of these gaps, i.e. if $P = 14$ GPa, the values of these gaps are 0.63 and 0.60 eV. At $14 < P \le 47$ GPa pressures, the Fermi level is immersed in the valence band. The corresponding value of the pseudogap at a pressure of $P = 47$ GPa is 1.80 eV. The magnetic moments of the supercell at pressures 0, 14 and 47 GPa are 4.56, 4.49 and 1.48 μ_B, respectively.

The results of calculations for an ideal ZnCoSe crystal are shown in Figures 6a, 6b. The ZnCoSe material exhibits semiconductor properties at all investigated pressure values for both spin orientations. For the spin up at pressures of 0, 20 and 49 GPa, the predicted optical gaps coincide with the fundamental ones and are equal to 1.15, 2.04 and 1.96 eV, respectively.

For spin down, at these pressure values, the optical gaps are 1.24, 2.11 and 1.71 eV, and the fundamental gaps equal 1.24 (direct at the Γ point), and two indirect gaps of 2.04 and 1.63 eV, respectively. The magnetic moments of the supercell are the same for all investigated pressure values and equal to 3 μ_B.

For a point-defect crystal, the data obtained are shown in Figures 6c, 6d. In the material with the vacancy for both values of the spin moment, the Fermi level is in the valence band. So, we can only talk about pseudo-gap. For spin up at pressures 0, 19 and 47 GPa, the values of pseudogaps equal to 1.12, 2.01 and 1.90 eV, and for spin down they are equal to 1.22, 1.74 and 1.31 eV, respectively. The magnetic moments of the supercell corresponding to pressures 0, 20 and 49 GPa are 2.26, 2.44 and 2.25 μ_B, respectively.

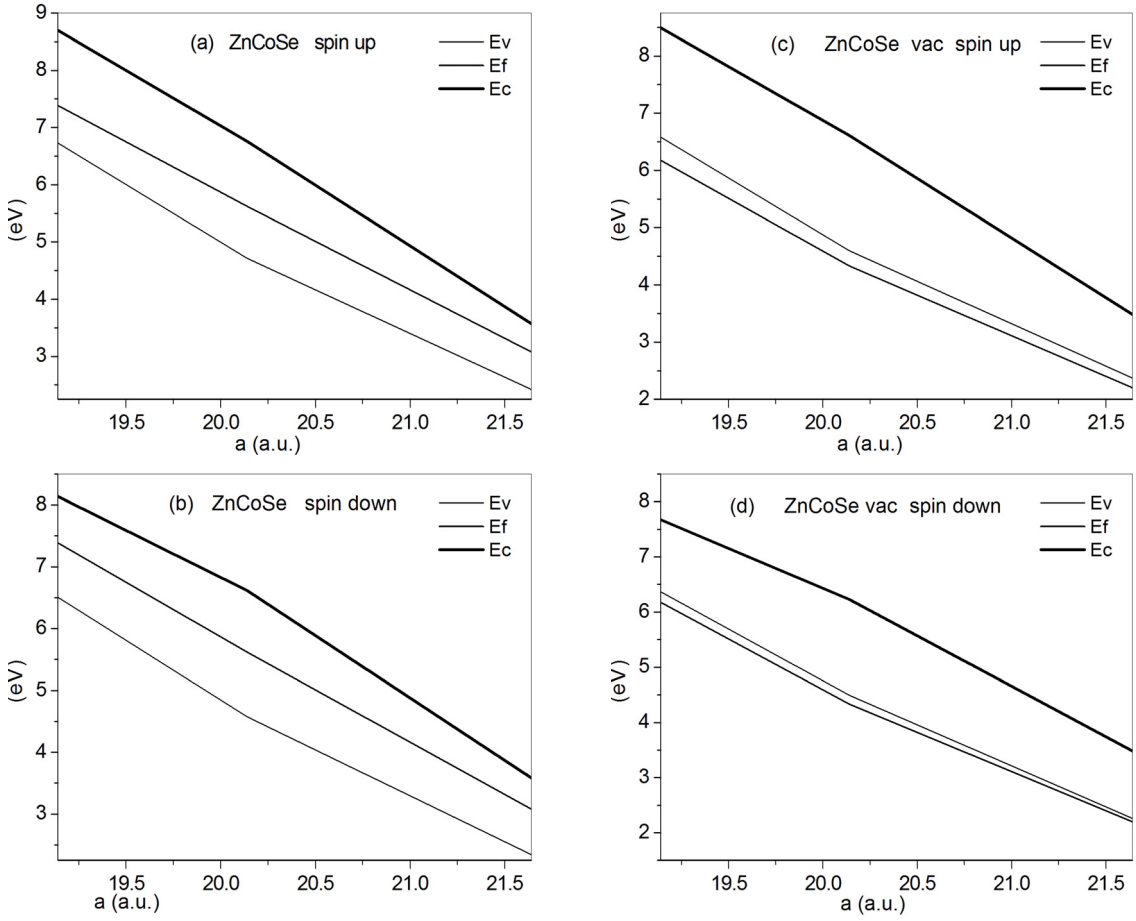

Figure 6. The spin-polarized electronic energy band parameters in the ZnCoSe material versus the 2×2×2 supercell lattice constant: top of valence band E_v, Fermi energy E_f and bottom of conduction band E_c.

The parameters of the electronic energy bands in an ideal ZnNiSe crystal are shown in Figures 7a and 7b. For the spin up, the Fermi level is inside the band gap, i.e. the material is a semiconductor. At pressure values of 0, 20 and 49 GPa, the optical and fundamental gaps are identical and equal to 1.19, 2.05 and 1.97 eV, respectively.

For spin down at $0 \le P \le 20$ GPa pressure values, the Fermi level is inside the band gap, i.e. the crystal is a semiconductor. At a pressure of $P = 0$, the band gap is 0.99 eV, at its value $P = 20$ GPa equals 1.24 eV. At higher $20 \le P \le 49$ GPa pressures, the Fermi level is in the valence band, and the pseudo gap corresponding to its largest value equals to 1.43 eV. The magnetic moments of the supercell are the same for the investigated pressure values and equal to 2 μ_B.

The introduction of the vacancy causes a radical change in the parameters of the electronic energy zones shown in Figures 7c, 7d. the magnetic moments of the supercell are 2.21, 2.15 and 1.94, respectively. For spin down at these pressures, the optical slits are 0.25, 0.29 and 0.21 eV, and the indirect fundamental slits are 0.19, 0.21 and 0.18 eV, respectively. The corresponding dependences of the parameters of the electronic energy zones are shown in Fig. 7d, allow to characterize the material as a narrow-band semiconductor.

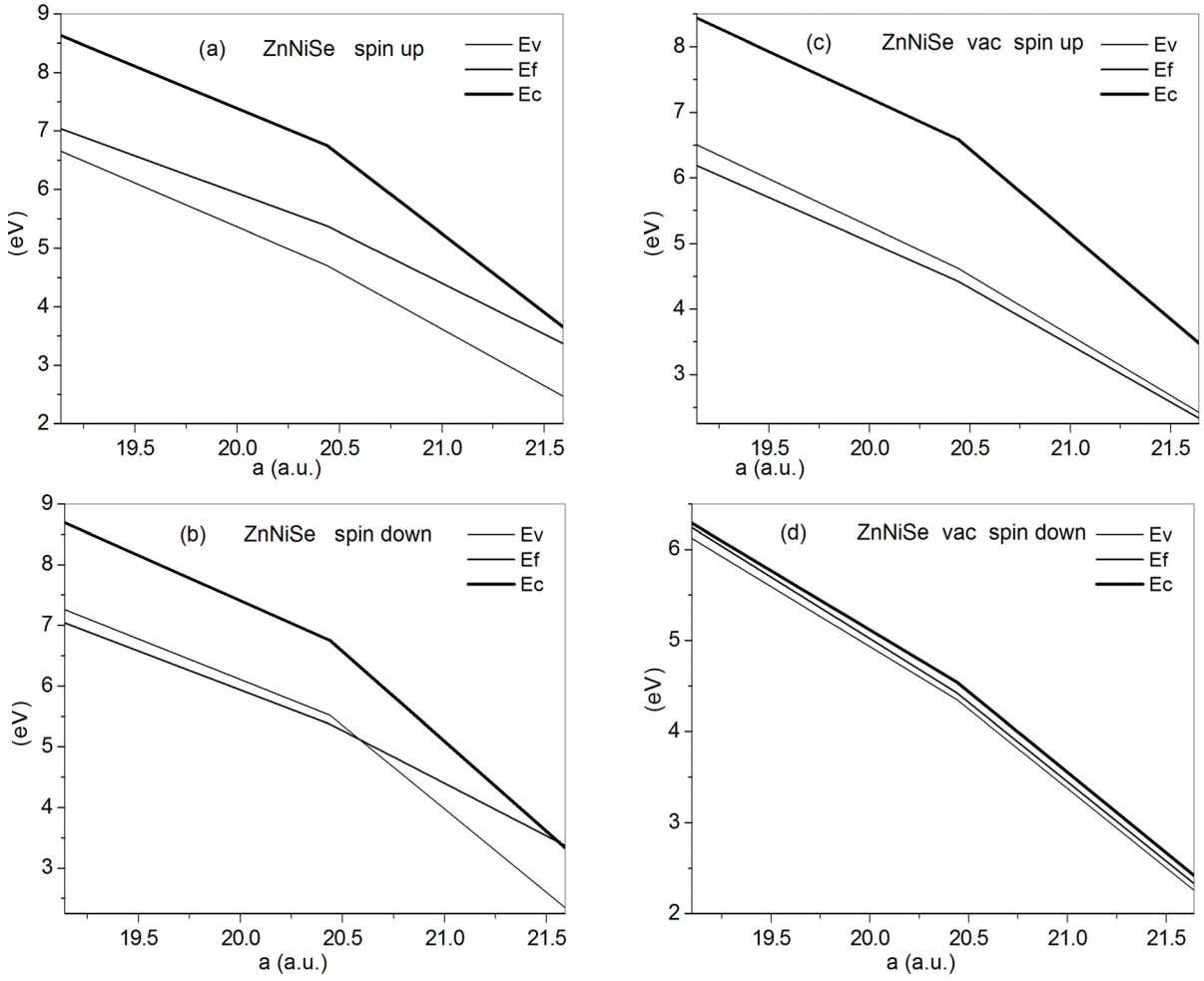

Figure 7. The spin-polarized electronic energy band parameters in the ZnNiSe material versus the 2×2×2 supercell lattice constant: top of valence band E_v, Fermi energy E_f and bottom of conduction band E_c.

In Figures 1–7, we observe a change in the dependence of the parameters of the electronic energy bands as a function of pressure (lattice parameter), which occurs at $20 \le P \le 21$ GPa pressure values. To reveal the nature of this behavior, let us consider the partial 3d DOS of transition elements. In Figures 8 a, b we notice a significant redistribution of the 3d DOS of the Ti atom caused by the increase in pressure. At pressure $P = 0$ we see the presence of 3d electrons of the Ti atom at the Fermi level for both values of the spin moment. This corresponds to the metallic state, as mentioned above. However, at a pressure of 21 GPa 3d states are absent at the Fermi level, and as noted above, the ideal ZnTiSe material exhibits semiconductor properties for both spin moments.

The magnetic moments on the Ti atom in an ideal ZnTiSe material at pressures of 0, 20, and 50 GPa are equal to 1.06, 1.00, and 0.92 μ_B, respectively. In the presence of a vacancy, their values vary greatly and at pressures of 0, 20 and 48 GPa are equal to 0.26, 0.01 and 0.00 μ_B, respectively.

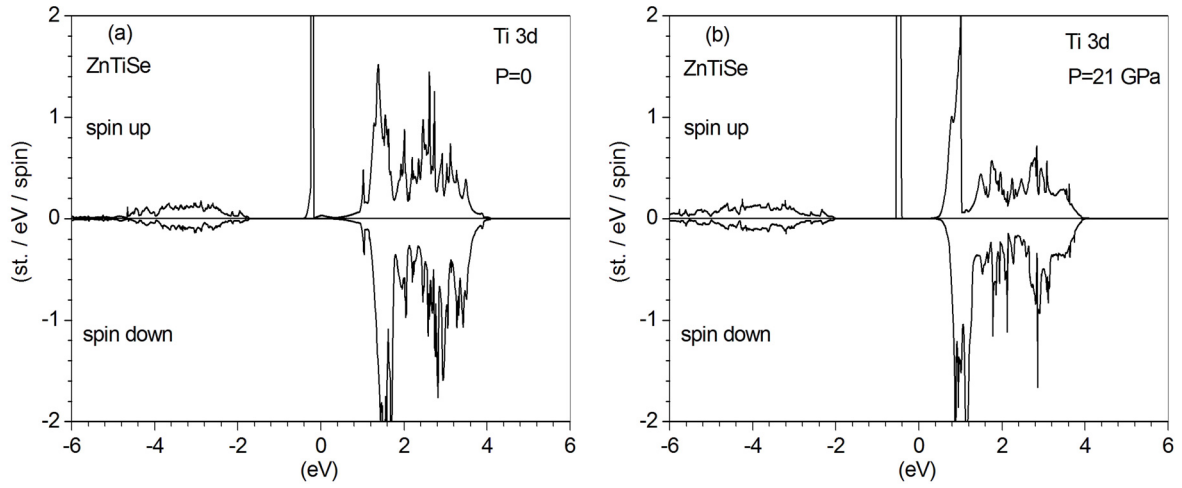

Figure 8. The spin-polarized DOS of the Ti 3d electrons in the ideal ZnTiSe material.

In Fig. 9 we also observe a significant redistribution of 3d electrons of the V atom caused by the increase in pressure. At a pressure $P = 0$ (Fig. 9 a) we see the presence of the V 3d electrons at the Fermi level for both spin orientations. However, at a pressure of 20 GPa (Fig. 9 b) we observe the presence of the V 3d electrons at the Fermi level only for the spin up.

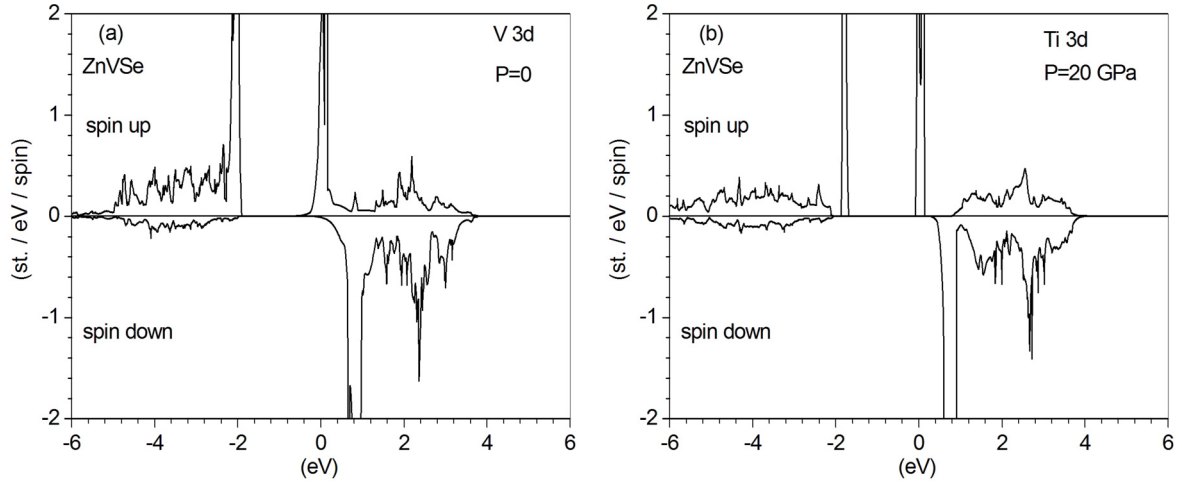

Figure 9. The spin-polarized DOS of the V 3d electrons in the ideal ZnVSe material.

The magnetic moments on the V atom in an ideal ZnVSe material at pressures of 0, 21, and 50 GPa are 1.72, 1.67, and 1.54 μ_B, respectively. If there is a vacancy, their values are much lower and at pressures 0, 20 and 48 GPa are equal to 1.44, 1.34 and 1.26 μ_B, respectively.

All the results of the electronic energy structure calculation were obtained here with the hybrid exchange-correlation functional PBE0. In this approach, it is possible to achieve a better positioning of 3d energy levels compared to that obtained using the usual GGA-PBE approximation [24].

We compare our results found in the PBE0 formalism for ZnCrSe and ZnFeSe materials with those obtained in the GGA-PBE approach [24]. From Figures 10 a, b we note that the Cr 3d states with higher energies and the spin up are located at the Fermi level, and those with lower energies are immersed in the valence band. This contradicts the results of [19], according to which the Fermi level and energy of 3d electrons are very close to the conduction band. For spin down approaches PBE0 and GGA-PBE [24] qualitatively give similar results, according to which 3d electrons form a conduction band. However, in the PBE0 approximation, the Fermi level is approximately 1.6 eV away from the lowest level of 3d electrons, whereas in the GGA-PBE formalism [24] this distance is approximately equal to 0.2 eV.

The results obtained for the ZnFeSe material are shown in Figures 10 c, d. In the PBE0 approach, we obtained the following results. For spin up, the smallest distance between the Fe 3d levels equals to 1.2 eV, whereas the GGA-PBE approximation [24] leads to its value of 0.6 eV. For spin down, part of the 3d states with lower energies is localized at the Fermi level, and the distance to the high-energy peak density of the 3d states is 1.6 eV. The same distance obtained in the GGA-PBE approach [24], approximately equal to 0.7 eV.

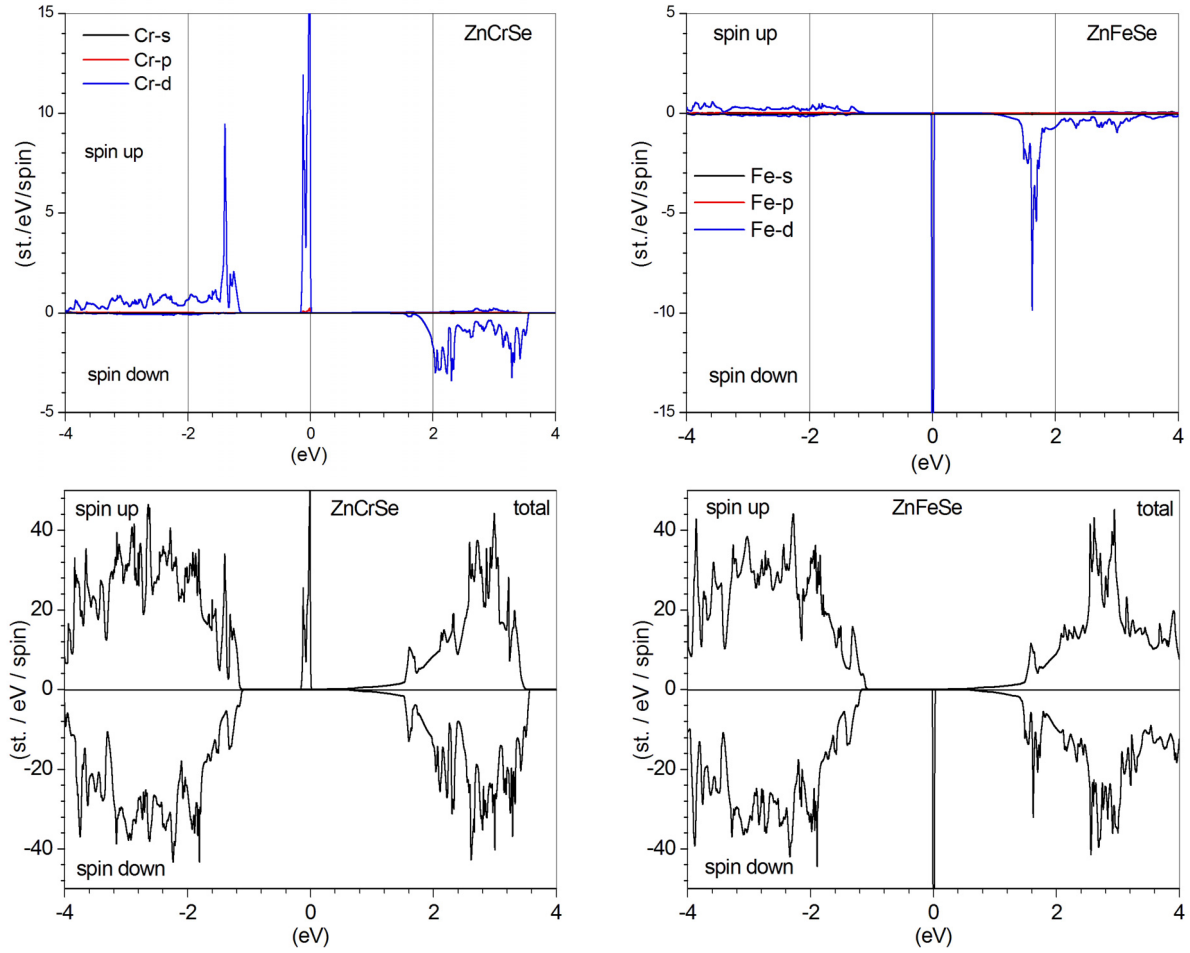

Figure 10. The spin-polarized partial DOS of the Cr (a) and Fe (c) atoms, and total DOS in the ideal materials ZnCrSe (c) and ZnFeSe (d).

Such differences between the parameters of the electronic energy bands obtained here in the PBE0 approach and in the GGA-PBE approximation [24], are explained by the fact that in the GGA-PBE formalism the electron density of s, p and d electrons is described by the same terms of the exchange-correlation functional. In the hybrid functional PBE0 s and p, electrons moving in wide energy zones are described in the GGA-PBE approximation. At the same time, the motion of 3d electrons in narrow energy zones with a high density of states is taken into account. The self-interaction error of 3d electrons is eliminated by adding the Hartree-Fock exchange potential, i.e. the PBE0 approach, which we apply here to all studied materials, has a significant advantage over the GGA-PBE approximation in describing the properties of materials containing d (f) electrons.

CONCLUSIONS

The electronic and magnetic properties in the ZnSe:T crystals have been evaluated for supercells $Zn_{31}T_1Se_{32}$ and $Zn_{30}v_1T_1Se_{32}$ under hydrostatic pressure. Here 3d transition atom T={Ti, V, Cr, Mn, Fe, Co, and Ni} substitutes the Zn one. The second supercells contain additionally a vacancy at Zn atom site. The strongly correlated 3d electrons are treated by means of the hybrid exchange-correlation functional PBE0, in which their self-interaction error is partly removed. It was found that under ambient conditions the materials $Zn_{31}Ti_1Se_{32}$ and $Zn_{31}V_1Se_{32}$ reveal metallic properties for both spin values. However, under the action of pressure, they become semiconductors. The introduction of a vacancy leads to a semiconductor state for all considered values of pressures and both spins in the $Zn_{30}v_1Ti_1Se_{32}$ material. But in the $Zn_{30}v_1V_1Se_{32}$ material the Fermi level is located in a valence band under low pressure, and it is a semiconductor under pressures $P > 21$ GPa. We have found that the combination of factors such as hydrostatic pressure and vacancy at the Zn atom site leads to a number of unexpected variety of the electronic and magnetic properties for the materials studied here. The results obtained in this work will be the basis for experiments to find effective materials for electronics application.

ORCID ID

Stepan V. Syrotyuk, https://orcid.org/0000-0003-4157-7351

REFERENCES

[1] Jen-Chuan Tung, Bang-Wun Lin, and Po-Liang Liu, ACS Omega, **10**(24), 8937 (2020), https://doi.org/10.3390/app10248937
[2] Fen Qiao, Rong Kang, Qichao Liang, Yongqing Cai, Jiming Bian, and Xiaoya Hou, ACS Omega **4**(7), 12271 (2019), https://doi.org/10.1021/acsomega.9b01539
[3] F. Trager, Lasers and Coherent Light Sources. In: *Springer Handbook of Lasers and Optics, 2nd ed.; T. Frank, Ed.* (Springer, Dordrecht, The Netherlands, 2012), **11**, pp. 749–750.
[4] S.B. Mirov, I.S. Moskalev, S. Vasilyev, V. Smolski, V.V. Fedorov, D. Martyshkin, J. Peppers , M. Mirov, A. Dergachev, and V. Gapontsev, IEEE Journal of Selected Topics in Quantum Electronics, **24**(5), 1601829 (2018), https://doi.org/10.1109/JSTQE.2018.2808284
[5] U. Demirbas, A. Sennaroglu, N. Vermeulen, H. Ottevaere, and H. Thienpont, *Proc. SPIE 6190, Solid State Lasers and Amplifiers II*, **61900A**(10), (2006), https://doi.org/10.1117/12.661725
[6] P.E. Blöchl, Phys. Rev. B. **50**, 17953 (1994), https://doi.org/10.1103/PhysRevB.50.17953
[7] M. Fuchs, M. Scheffler, Comput. Phys. Commun. **119**, 67 (1999).
[8] G.K.H. Madsen, P. Blaha, K. Schwarz, E. Sjöstedt, and Lars Nordström, Phys. Rev. B. **64**, 195134 (2001), https://doi.org/10.1103/PhysRevB.64.195134
[9] M. Ernzerhof, and G.E. Scuseria, J. Chem. Phys. **110**, 5029 (1999), https://doi.org/10.1063/1.478401
[10] P. Novák, J. Kunes, L. Chaput, and W.E. Pickett, Phys. Status Solidi B, **243**(3), 563 (2006), https://doi.org/10.1002/pssb.200541371
[11] E. Tran, P. Blaha, K. Schwarz, and P. Novák, Phys. Rev. B, **74**, 155108 (2006), https://doi.org/10.1103/PhysRevB. 74.155108
[12] J.P. Perdew, K. Burke, and M. Ernzerhof, Phys. Rev. Letters, **77**(18), 3865 (1996), https://doi.org/10.1103/PhysRevLett. 77.3865
[13] Y. Klysko, and S. Syrotyuk, Ukr. J. Phys. **66**(1), 55 (2021), https://ujp.bitp.kiev.ua/index.php/ujp/article/view/2019493
[14] S.V. Syrotyuk, and Yu.V. Klysko, Condens. Matter Phys. **23**(3), 33703 (2020), https://doi.org/10.5488/CMP.23.33703)
[15] Ya.M. Chornodolskyy, V.O. Karnaushenko, V.V. Vistovskyy, S.V. Syrotyuk, A.V. Gektin, and A.S. Voloshinovskii, Journal of Luminescence **237**, 118147 (2021), https://doi.org/10.1016/j.jlumin.2021.118147
[16] S.V. Syrotyuk, Physics and Chemistry of Solid State, **21**(4), 695 (2020), https://doi.org/10.15330/pcss.21.4.695-699)
[17] S.V. Syrotyuk, and O.P. Malyk, J. Nano- Electron. Phys. **11**(6), 06018 (2019), https://doi.org/10.21272/jnep.11(6).06018
[18] S.V. Syrotyuk, and O.P. Malyk, J. Nano- Electron. Phys. **11**(1), 01009 (2019), https://doi.org/10.21272/jnep.11(1).01009
[19] R.Yu. Petrus, H.A. Ilchuk, V.M. Sklyarchuk, A.I. Kashuba, I.V. Semkiv, and E.O. Zmiiovska, J. Nano- Electron. Phys. **10**, 06042 (2018), https://doi.org/10.21272/jnep.10(6).06042
[20] S.V. Syrotyuk, Metallofiz. Noveishie Tekhnol. **43**(4), 541 (2021), https://doi.org/10.15407/mfint.43.04.0541
[21] X. Gonze, F. Jollet, F. Abreu Araujo, D. Adams, B. Amadon, T. Applencourt, C. Audouze, et al, Comput. Phys. Commun. **205**, 106 (2016), https://doi.org/10.1016/j.cpc.2016.04.003
[22] N.A.W. Holzwarth, A.R. Tackett, and G.E. Matthews, Comput. Phys. Commun. **135**, 329 (2001), https://doi.org/10.1016/S0010-4655(00)00244-7)
[23] A.R. Tackett, N.A.W. Holzwarth, and G.E. Matthews, Comput. Phys. Commun. **135**, 348 (2001), https://doi.org/10.1016/S0010-4655(00)00241-1
[24] Y. Zhang, G. Feng, and S. Zhou, Proc. SPIE 9920, Active Photonic Materials VIII, 99200L (16 September 2016); SPIE Nanoscience + Engineering, 2016, San Diego, California, United States, https://doi.org/10.1117/12.2236152

ВПЛИВ ГІДРОСТАТИЧНОГО ТИСКУ І КАТІОННОЇ ВАКАНСІЇ НА ЕЛЕКТРОННІ ТА МАГНІТНІ ВЛАСТИВОСТІ КРИСТАЛІВ ZnSe:T (T = Ti, V, Cr, Mn, Fe, Co, Ni)

Степан В. Сиротюк

Національний університет "Львівська політехніка", 79013 Львів Україна

Параметри поляризованого за спіном електронного енергетичного спектру кристалів ZnSe: T (T = Ti, V, Cr, Mn, Fe, Co, Ni) вивчаються на основі надкомірки 2×2×2, побудованої на базі кристала ZnSe зі структурою сфалериту. Надкомірка містить 64 атоми, з яких один атом Zn заміщується перехідним 3d елементом T. Перший етап даного дослідження полягає в розрахунку в ідеальному матеріалі ZnTSe залежних від зовнішнього гідростатичного тиску параметрів електронних енергетичних зон. На другому етапі досліджується вплив тиску на значення параметрів електронного енергетичного спектру матеріалів ZnTSe з урахуванням вакансії на вузлі атома Zn. Розрахунки виконані за допомогою програми Abinit. Для кращого опису сильно скорельованих 3d електронів елемента T був застосований гібридний обмінно-кореляційний функціонал PBE0 з домішкою обмінного потенціала Хартрі-Фока, у якому відсутня самодія цих електронів. На основі отриманих електронних густин, поляризованих за спіном, були визначені також і магнітні моменти надкомірок. Виявлено значний вплив тиску на параметри електронних енергетичних зон. Так, ідеальний матеріал ZnTiSe за нульового тиску є металом для обидох значень спіна, але під дією тиску він стає напівпровідником. Цей же матеріал з точковим дефектом, тобто вакансією на вузлі атома Zn, виявляє властивості напівпровідника для обидвох орієнтацій спіна за нульового тиску. Виявлено, що вакансії докорінно змінюють параметри електронних енергетичних зон. Магнітні моменти надкомірки, як інтегральні величини поляризованих за спіном густин електронних станів, також відображають ці зміни. Так, у матеріалі ZnTiSe без дефектів магнітні моменти надкомірки становлять 1.92, 2.0 та 2.0 μ_B , за тисків 0, 21 та 50 GPa, тоді як тому ж матеріалі з вакансією відповідні значення становлять 0.39, 0.02 та 0.36 μ_B . Ідеальний матеріал ZnVSe за нульового тиску також є металом для обидвох значень спінового моменту, але за наявності катіонної вакансії він є характеризується псевдощілиною, оскільки рівень Фермі локалізований у верхній частині валентної зони. Ідеальні кристали ZnFeSe та ZnNiSe характеризуються подібними залежностями від тиску параметрів електронних енергетичних зон для обидвох спінів. Однак ці ж матеріали з катіонною вакансією характеризуються для спінів вгору рівнем Фермі, зануреним у валентну зону.

Ключові слова: ZnSe, домішка 3d, катіонна вакансія, електронні властивості, спін, магнітний момент, сильні кореляції, гібридний функціонал.